

# PULSATIONAL INSTABILITY OF YELLOW HYPERGIANTS

Yu. A. Fadeyev<sup>1</sup>

*Institute of Astronomy, Russian Academy of Sciences, Pyatnitskaya ul. 48, Moscow, 109017  
Russia*

Received

**Abstract** — Instability of population I ( $X = 0.7$ ,  $Z = 0.02$ ) massive stars against radial oscillations during the post-main-sequence gravitational contraction of the helium core is investigated. Initial stellar masses are in the range  $65M_{\odot} \leq M_{\text{ZAMS}} \leq 90M_{\odot}$ . In hydrodynamic computations of self-exciting stellar oscillations we assumed that energy transfer in the envelope of the pulsating star is due to radiative heat conduction and convection. The convective heat transfer was treated in the framework of the theory of time-dependent turbulent convection. During evolutionary expansion of outer layers after hydrogen exhaustion in the stellar core the star is shown to be unstable against radial oscillations while its effective temperature is  $T_{\text{eff}} > 6700\text{K}$  for  $M_{\text{ZAMS}} = 65M_{\odot}$  and  $T_{\text{eff}} > 7200\text{K}$  for  $M_{\text{ZAMS}} = 90M_{\odot}$ . Pulsational instability is due to the  $\kappa$ -mechanism in helium ionization zones and at lower effective temperature oscillations decay because of significantly increasing convection. The upper limit of the period of radial pulsations on this stage of evolution does not exceed  $\approx 200$  day. Radial oscillations of the hypergiant resume during evolutionary contraction of outer layers when the effective temperature is  $T_{\text{eff}} > 7300\text{K}$  for  $M_{\text{ZAMS}} = 65M_{\odot}$  and  $T_{\text{eff}} > 7600\text{K}$  for  $M_{\text{ZAMS}} = 90M_{\odot}$ . Initially radial oscillations are due to instability of the first overtone and transition to fundamental mode pulsations takes place at higher effective temperatures ( $T_{\text{eff}} > 7700\text{K}$  for  $M_{\text{ZAMS}} = 65M_{\odot}$  and  $T_{\text{eff}} > 8200\text{K}$  for  $M_{\text{ZAMS}} = 90M_{\odot}$ ). The upper limit of the period of radial oscillations of evolving blueward yellow hypergiants does not exceed  $\approx 130$  day. Thus, yellow hypergiants are stable against radial stellar pulsations during the major part of their evolutionary stage.

Keywords: *stars: variable and peculiar.*

---

<sup>1</sup>E-mail: fadeyev@inasan.ru

# 1 INTRODUCTION

More than a half-century ago Feast and Thackeray (1956) pointed out the significant scatter in luminosities (up to 7 magnitudes) of supergiants of the Large Magellanic Cloud. The most luminous stars of this sample of spectral types F and G the authors of this work named as super-supergiants. Later the name super-supergiant was changed to a hypergiant and the luminosity class of such objects was denoted as Ia<sup>+</sup> or Ia0 (de Jager 1980). The high luminosity and the low surface gravity favour the strong stellar wind, so that as one more criterion of the hypergiant one should consider the widely broadened emission and absorption lines. Evolutionary status of yellow hypergiants are thought to be that they are the post-main-sequence massive stars (i.e. with initial masses  $M_{\text{ZAMS}} > 40M_{\odot}$ ) undergoing gravitational contraction of the helium core (Meynet et al. 1994; Stothers and Chin 1996; Langer et al. 2007).

Yellow hypergiants are variable objects but the common point of view on nature of their variability does not exist yet. Stothers and Chin (1996, 2001) showed that outer layers of hypergiants might be dynamically unstable because the adiabatic exponent becomes smaller its critical value ( $\Gamma_1 < 4/3$ ) due to partial ionization of helium and the large contribution of radiation pressure. Outer layers of the hypergiant can be unstable also due to convection in the hydrogen and helium ionization zones. De Jager and Nieuwenhuijzen(1997) and de Jager et al. (2001) estimated that the gradient of the turbulent pressure in subphotospheric layers might reduce the effective gravity almost to zero. However this conclusion was not confirmed by Stothers (2003) who showed that the turbulent pressure is insignificant and this effect can be neglected.

Together with irregular enhancements of the stellar wind some yellow hypergiants show cyclic light variations. The most remarkable example is  $\rho$  Cas with light amplitude of a few tenths of a magnitude and the period of order of several hundred days (Arellano Ferro 1985; Sheffer and Lambert 1986; Zsoldos and Percy 1991; Lobel et al. 1994, 1998). Most of these authors mentioned the fact that cyclic light variations of  $\rho$  Cas are very similar to those of pulsating stars. Moreover, near-IR CO line profiles demonstrate splitting similar to that observed in pulsating supergiants of intermediate spectral types such as RV Tau and R CrB variables (Gorlova et al. 2006). At the same time there seems to be a contradiction with pulsation hypothesis because light variations with period of  $\approx 500$  day cannot be explained in terms of radial stellar pulsations for typical masses and radii of yellow hypergiants (Sheffer and Lambert 1986). Here one should be noted that no studies of pulsational instability of yellow hypergiants have been done yet, so that disussion of their photometric variability in terms of stellar pulsations remains hypothetical.

As shown in our previous paper (Fadeyev 2011) the population I stars ( $Z \geq 0.02$ ) with initial mass  $M_{\text{ZAMS}} > 60M_{\odot}$  become unstable against radial oscillations during the main-

sequence evolutionary stage and they pulsate at least up to hydrogen exhaustion in the stellar core. The goal of the present study is to consider the pulsation properties of massive stars during the later evolutionary stage of gravitational contraction of the helium core and to determine the role of radial stellar pulsations in variability of yellow hypergiants.

## 2 THE METHOD OF COMPUTATIONS

The methods used to compute the stellar evolution and self-exciting radial stellar oscillations were described in our previous papers (Fadeyev 2007, 2008a, 2008b, 2010, 2011), so that below we outline the most important improvements employed in hydrodynamic calculations of the present work. In studies of radial pulsations of Wolf-Rayet stars (Fadeyev 2007, 2008a, 2008b) and LBV-stars (Fadeyev 2010) the hydrodynamic computations were done in assumption of radiation transfer without convection. Bearing in mind complete ionization of hydrogen and helium in outer layers of these stars such an approach seems to be appropriate. In calculations of nonlinear pulsations of massive main-sequence stars with effective temperatures  $T_{\text{eff}} > 2 \times 10^4 \text{K}$  (Fadeyev 2011) the energy transport was assumed to be due to radiation and convection. The region of convective heat transfer encompasses the zone of the iron Z-bump ( $T \sim 2 \times 10^5 \text{K}$ ) and convection was treated in the framework of the local steady-state mixing length theory (Böhm-Vitense 1958). However in outer layers (i.e. in hydrogen and helium ionization zones) of yellow hypergiants with effective temperatures  $T_{\text{eff}} < 10^4 \text{K}$  the significant fraction of energy is transported by convection and interaction of convective elements with pulsation motions should be taken into account because of the large pulsation amplitude. To this end in the present study we employ the equations of time-dependent turbulent convection obtained by Kuhfuss (1986) from Navier-Stokes equations written for spherical geometry.

For spherically-symmetric motions the Lagrangean mass coordinate  $M_r$  and the radius  $r$  are related by continuity equation  $dM_r = 4\pi r^2 \rho dr$ , where  $\rho$  is the gas density. Equation of motion describing the radial gas flow velocity  $U$  as a function of time  $t$  is

$$\frac{\partial U}{\partial t} = -4\pi r^2 \frac{\partial(P + P_t + P_v)}{\partial M_r} - \frac{GM_r}{r^2}, \quad (1)$$

where  $P$  is the total thermodynamic (gas plus radiation) pressure,  $P_t$  is the turbulent pressure,  $P_v$  is the turbulent viscous pressure,  $G$  is the Newtonian gravitational constant. The energy conservation equation is

$$\frac{\partial(E + E_t)}{\partial t} + (P + P_t + P_v) \frac{\partial}{\partial t} \left( \frac{1}{\rho} \right) = -\frac{1}{\rho} \nabla \cdot \mathbf{F}, \quad (2)$$

where  $E$  is the specific internal energy (the sum of the translational, excitation, ionization and radiation energies per gram of material),  $E_t$  is the root-mean specific turbulent energy,  $\mathbf{F} = \mathbf{F}_{\text{rad}} + \mathbf{F}_c + \mathbf{F}_t$  is the total flux, that is the sum of the radiative, convective (enthalpy) and turbulent (kinetic energy of convective elements) fluxes.

Additionally we write the equation for conservation of the turbulent energy

$$\frac{\partial E_t}{\partial t} + (P_t + P_v) \frac{\partial}{\partial t} \left( \frac{1}{\rho} \right) = S_t - D_t - \frac{1}{\rho} \nabla \cdot \mathbf{F}_t, \quad (3)$$

where  $D_t$  is dissipation of turbulent energy due to molecular viscosity and  $S_t$  is the source or sink of the turbulent energy due to buoyancy forces. In the isotropic medium the turbulent pressure  $P_t$ , the mean turbulent energy  $E_t$  and the root-mean speed of convective elements  $v_c$  are related by

$$P_t = \frac{2}{3} \rho E_t = \rho v_c^2. \quad (4)$$

Expressions for other quantities in equations (1) – (3) can be found in papers by Wuchterl and Feuchtinger (1998), Olivier and Wood (2005), Smolec and Moskalik (2008).

The numerical solution of equations (1) – (3) was done with difference equations of the second-order accuracy in both the spatial coordinate  $M_r$  and the time  $t$ . The equation of motion (1) was solved with the explicit finite-difference method, whereas equations (2) and (3) were treated implicitly using the Crank–Nicholson scheme (see, e.g., Richtmyer and Morton 1967). Thus, at each step of integration with respect to time  $t$  the temperature  $T$  and the specific turbulent energy  $E_t$  are determined for all Lagrangean mass zones of the hydrodynamic model from iterative solution of linearized difference energy equations.

For the inner boundary condition we employed the assumption of the rigid sphere with the time-independent flux:

$$\frac{\partial r_0}{\partial t} = \frac{\partial L_0}{\partial t} = 0, \quad (5)$$

where  $r_0$  and  $L_0$  are the radius and luminosity at the inner boundary. The gas temperature at the inner boundary is  $T < 10^6 \text{K}$  and therefore the thermonuclear energy generation within the pulsating envelope can be neglected. In hydrodynamic calculations the luminosity at the inner boundary  $L_0$  was treated as the initial parameter of the hydrodynamic model determined from computations of stellar evolution. It should be noted that for the sake of stability of the numerical solution the inner boundary condition of the energy equation was written in assumption of radiation heat conduction. Therefore, the inner boundary of the hydrodynamical model is always below the iron Z-bump convection zone ( $T \sim 2 \times 10^5 \text{K}$ ). For models considered in the present study the radius of the inner boundary is  $r_0 \lesssim 3 \times 10^{-2} R$ , where  $R$  is the equilibrium radius of the outer boundary.

At the evolutionary stage of the yellow hypergiant the stellar mass is about a half of its initial mass and in the outer layers of the star there is the negative gradient of the mean molecular weight. The spatial inhomogeneity of the chemical composition is due to diminution of the both stellar mass and mass of convective core during the main-sequence hydrogen burning. However the mass of outer pulsating layers of the hypergiant is enough small in comparison with stellar mass ( $M_{\text{env}} < 10^{-3} M$ ), so that effects of inhomogeneity of chemical composition with respect to spatial coordinate remain always negligible.

### 3 RESULTS OF COMPUTATIONS

#### 3.1 STELLAR EVOLUTION

Yellow hypergiants are on the short evolutionary stage of gravitational contraction of the helium core during of which the star evolves along the loop in the Hertzsprung–Russell (HR) diagram and its effective temperature becomes as low as  $4 \times 10^3 \text{K} \lesssim T_{\text{eff}} \lesssim 5 \times 10^3 \text{K}$ . The parts of the evolutionary tracks of stars with effective temperatures  $T_{\text{eff}} \leq 10^4 \text{K}$  and initial masses  $M_{\text{ZAMS}} = 65M_{\odot}$  and  $90M_{\odot}$  are shown in Fig. 1(a). The time of evolution along the shown parts of the tracks ranges from  $\approx 10^4$  yr ( $M_{\text{ZAMS}} = 90M_{\odot}$ ) to  $\approx 2 \times 10^4$  yr ( $M_{\text{ZAMS}} = 65M_{\odot}$ ).

During evolutionary expansion of outer layers when the stellar effective temperature is  $T_{\text{eff}} = 10^4 \text{K}$  (the initial point of the tracks in Fig. 1(a)) the principal energy source is gravitational contraction of the helium core. For example, the ratio of central values of the thermonuclear energy generation rate  $\varepsilon_c$  (these are mostly reactions of the 3- $\alpha$  process) and the gravitational energy release ranges from  $\alpha_c = \varepsilon_c / (-T_c \partial S_c / \partial t) \approx 7 \times 10^{-3}$  for  $M_{\text{ZAMS}} = 65M_{\odot}$  to  $\alpha_c \approx 0.05$  for  $M_{\text{ZAMS}} = 90M_{\odot}$ . Here  $T_c$  and  $S_c$  are the temperature and specific entropy in the center of the star. This ratio gradually increases with time and at the turning point of the track is  $\alpha_c \approx 10^2$  independently of  $M_{\text{ZAMS}}$ . At ending points of the tracks shown in Fig. 1(a) this ratio is  $\alpha_c \approx 300$  for  $M_{\text{ZAMS}} = 65M_{\odot}$  and  $\alpha_c \approx 10^3$  for  $M_{\text{ZAMS}} = 90M_{\odot}$ .

Gradual decrease of the role of gravitational contraction in the total stellar energy production leads to deceleration of the evolutionary movement along the track. This effect is illustrated in Fig 1(b), where for tracks in Fig 1(a) we give the plots of the rate of effective temperature change  $d \ln T_{\text{eff}} / dt$ . For example, at  $T_{\text{eff}} \approx 7 \cdot 10^3 \text{K}$  the rate of the redward evolution in the HR diagram about five times of that in the opposite direction at the same effective temperature. Thus, the probability to observe the yellow hypergiant with increasing effective temperature is significantly higher than that to observe the hypergiant with expanding outer layers. Nevertheless in our study we consider the pulsation properties of hypergiants with effective temperatures  $T_{\text{eff}} \leq 10^4 \text{K}$  independently of direction of their evolution in the HR diagram.

#### 3.2 PULSATIONS OF YELLOW HYPERGIANTS

The study of self-exciting stellar oscillations implies solution of the Cauchy problem for equations (1) – (3) with initial conditions corresponding to the hydrostatic and thermal ( $\nabla \cdot \mathbf{F} = 0$ ) equilibrium. To this end we used some stellar models of preliminary computed evolutionary sequences. Stability of the star against radial oscillations is determined from integration of the equations of hydrodynamics with respect to time  $t$ . In the case of pulsational instability the solution describes the exponentially growing oscillation amplitude with following transition to the limit cycle oscillations. The main quantities characterizing the limit cycle are the period  $\Pi$

and the amplitude of the radial displacement of the outer boundary  $\Delta R$  expressed in units of the equilibrium stellar radius  $R$ .

In Fig. 2 the plots of  $\Delta R/R$  and  $\Pi$  as a function of  $T_{\text{eff}}$  are shown for the evolutionary sequence of models with initial mass  $M_{\text{ZAMS}} = 65M_{\odot}$ . As in the HR diagram the effective temperature increases from right to left. The dashed lines correspond to the evolutionary expansion of outer layers of the star, that is to decrease of the effective temperature, whereas solid lines correspond to their contraction.

Radial oscillations of the hypergiant at the initial point of the evolutionary track ( $T_{\text{eff}} = 10^4\text{K}$ ) are driven by the layers of the iron Z-bump ( $T \sim 2 \times 10^5\text{K}$ ) and by helium ionization zones locating closer to the surface. The role of the iron Z-bump in pulsational instability decreases with decreasing effective temperature because of diminution of the relative radius  $r/R$  and the amplitude of radial displacement  $\Delta r$  in these layers. That is why the evolutionary decrease of the effective temperature is accompanied by decreasing pulsation amplitude  $\Delta R/R$ . This conclusion is illustrated in Fig. 3 where for two hydrodynamical models with effective temperatures  $T_{\text{eff}} = 10^4\text{K}$  and  $T_{\text{eff}} = 6800\text{K}$  we show the radial dependencies of the mechanical work over a closed thermodynamic cycle:

$$W_j = \frac{\Delta M_j}{|W|} \oint P_j dV_j. \quad (6)$$

Here  $\Delta M_j$  is the mass of the  $j$ -th Lagrangean interval,  $P_j$  is the sum of the thermodynamic pressure and turbulent pressure,  $V_j$  is the specific volume,

$$|W| = \sum_{j=1}^N \Delta M_j \oint |P_j dV_j| \quad (7)$$

is the normalizing coefficient,  $N$  is the number of Lagrangean zones in the hydrodynamical model. Depending on the stellar structure the hydrodynamic computations were done with  $500 \leq N \leq 1000$ .

As seen in Fig. 3 the evolutionary decrease of effective temperature from  $10^4\text{K}$  to  $6800\text{K}$  is accompanied by decrease of the relative radius of the layer with maximum mechanical work  $W_j$  at the iron Z-bump from  $r/R \approx 0.3$  to  $r/R \approx 0.15$ . At the same time the contribution of the iron Z-bump zone into the positive mechanical work decreases from 0.43 to 0.1, so that near the boundary of the pulsational instability radial pulsations are driven mostly in the helium ionization zones. Here we have to note that the plots of the mechanical work  $W_j$  in Fig. 3 are shown as a function of the equilibrium relative radius  $r/R$ , whereas the mechanical work of a group of mass zones is determined from integration with respect to mass coordinate  $M_r$ .

Evolutionary expansion of the hypergiant outer layers is accompanied by increase of convection in the helium ionization zones, so that for  $T_{\text{eff}} \lesssim 6700\text{K}$  the radial oscillations decay due to large decrease of the radiative flux in ionization zones. Recommencement of radial oscillations

becomes possible after the turn of the evolutionary track when the effective temperature rises up to  $T_{\text{eff}} \gtrsim 7300\text{K}$ . Pulsational properties of the hypergiant during evolutionary contraction of outer layers are illustrated in Fig. 4, where radial dependencies of the mechanical work over a closed thermodynamic cycle are shown for hydrodynamical models with  $T_{\text{eff}} = 7400\text{K}$  and  $10^4\text{K}$ .

The star of effective temperature  $T_{\text{eff}} = 7400\text{K}$  with contracting outer layers locates near the boundary of the pulsational instability region. In comparison with the hypergiant of the same effective temperature but on the preceding evolutionary stage of expanding outer layers (the luminosity and the surface mass fraction of helium are  $L = 1.033 \times 10^6 L_{\odot}$  and  $Y_s = 0.74$ ) the star has a somewhat higher luminosity and perceptibly higher surface abundance of helium:  $L = 1.085 \times 10^6 L_{\odot}$ ,  $Y_s = 0.88$ . The higher helium abundance leads to a larger opacity of stellar material and to stronger convection in the helium ionization zones, so that the boundary of the pulsation instability moves to somewhat higher effective temperatures in comparison with hypergiants undergoing expansion of outer layers.

Pulsational instability of the hypergiant during evolutionary contraction of its outer layers is due to the  $\kappa$ -mechanism in the helium ionization zones. The radial dependence of the mechanical work over a closed thermodynamic cycle for the model near the boundary of instability region is shown in Fig. 4 by the dashed line. Two prominent positive maxima on the plot correspond to the zones of the first ionization and second ionization of helium, whereas the contribution of the iron Z-bump zone into the positive mechanical work does not exceed 6%. During further evolution with increasing effective temperature the role of the iron Z-bump zone remains insignificant and at  $T_{\text{eff}} = 10^4\text{K}$  its contribution into the total positive mechanical work remain less than 8%.

Of greatest interest in comparison with observations is the pulsation period  $\Pi$ . During the evolutionary expansion of outer layers in the hypergiant with initial mass  $M_{\text{ZAMS}} = 65M_{\odot}$  the radial pulsations are due to instability of the fundamental mode and as seen in Fig. 2(b) the period gradually increases with decreasing  $T_{\text{eff}}$  up to the instability boundary. During movement along the track in the opposite direction the radial oscillations resume at effective temperature  $T_{\text{eff}} = 7400\text{K}$ . For  $T_{\text{eff}} < 7700\text{K}$  the star pulsates in the first overtone and the period of the contracting hypergiant is significantly shorter than that of the expanding hypergiant with the same effective temperature. Transition of radial pulsations from the first overtone to the fundamental mode takes place at effective temperature  $T_{\text{eff}} \approx 7700\text{K}$  and is revealed by a jump in plots of the surface amplitude  $\Delta R/R$  and period  $\Pi$  (see Fig. 2).

To compare the hypergiant pulsation properties at evolutionary stages of expansion and contraction we give in Fig. 5 the plots of the gas flow velocity at the outer boundary  $U$  and the light in V band  $m_V$  for two hydrodynamical models with initial mass  $M_{\text{ZAMS}} = 65M_{\odot}$  and effective temperature  $T_{\text{eff}} = 7500\text{K}$ . The significant difference in amplitudes of velocity and

light curves is due to the fact that evolutionary contracting hypergiant pulsates in the first overtone, whereas during evolutionary expansion the hypergiant pulsates in the fundamental mode. However at effective temperatures  $T_{\text{eff}} > 7700\text{K}$  the difference in pulsational properties becomes insignificant (see Fig. 6) because on both evolutionary stages the hypergiant pulsates in the fundamental mode.

Above we discussed results of hydrodynamic calculations for stars with initial mass  $M_{\text{ZAMS}} = 65M_{\odot}$ . Hypergiants with larger initial mass have a higher helium abundance in their outer layers because of the more massive convective core and the stronger stellar wind during the main-sequence evolutionary stage. Therefore in more massive hypergiants with  $T_{\text{eff}} < 10^4\text{K}$  the convection in helium ionization zones is stronger and the boundary of the pulsation instability region corresponds to higher effective temperatures. For example, in stars with initial mass  $M_{\text{ZAMS}} = 90M_{\odot}$  the radial pulsations cease during evolutionary expansion of outer layers at effective temperature  $T_{\text{eff}} \approx 7200\text{K}$  and resume during evolutionary contraction at  $T_{\text{eff}} \approx 7600\text{K}$ .

In Fig. 7 the amplitude of the radial displacement of the outer boundary  $\Delta R/R$  and the pulsation period  $\Pi$  are shown as a function of effective temperature for hypergiants with initial mass  $M_{\text{ZAMS}} = 90M_{\odot}$ . With approaching the boundary of pulsational instability during the evolutionary expansion of outer layers the mode of radial oscillations changes and hypergiants with effective temperature  $T_{\text{eff}} < 7800\text{K}$  pulsate in the first overtone. Therefore, the maximum period of radially pulsating hypergiant with initial mass  $M_{\text{ZAMS}} = 90M_{\odot}$  does not exceed 150 day. During movement along the track in the opposite direction the radial oscillations resume in the first overtone at effective temperature  $T_{\text{eff}} \approx 7700\text{K}$  and at  $T_{\text{eff}} \gtrsim 8400\text{K}$  the star oscillates in the fundamental mode.

The main properties of some hydrodynamic models of radially pulsating hypergiants with initial masses  $M_{\text{ZAMS}} = 65M_{\odot}$  and  $90M_{\odot}$  are summarized in the table. All models are represented in four sequences depending on the initial stellar mass  $M_{\text{ZAMS}}$  and direction of movement in the HR diagram. The stellar mass  $M$ , the luminosity  $L$  and the surface fractional mass abundance of hydrogen  $X_{\text{s}}$  approximately do not change within each sequence and therefore are given only for the first model of the sequence. The luminosity  $L$  and effective temperature  $T_{\text{eff}}$  correspond to the initial hydrostatic equilibrium,  $\Pi$  and  $Q$  are the pulsation period and pulsation constant in days,  $k$  is the order of the pulsation mode ( $k = 0$  for the fundamental mode and  $k = 1$  for the first overtone). The rate of period change  $\dot{\Pi}/\Pi = d \ln \Pi / dt$  was evaluated from the second-order numerical differentiation with respect to age of the stellar evolution model used as initial conditions in hydrodynamic calculations. Thus, to evaluate the rate of period change we had to compute two additional hydrodynamical models. In the table we give only most reliable estimates of this quantity. The amplitude of the radial displacement of the outer boundary  $\Delta R$  expressed in units of the initial equilibrium radius  $R$  and the amplitude of the radial velocity at the outer boundary  $\Delta U$  are given in last two columns of the table.



## 4 CONCLUSIONS

Results of hydrodynamic calculations described in the present paper allow us to conclude that radial oscillations is rather a short-term phenomenon in the life of yellow hypergiants. For example, hypergiants with initial masses  $65M_{\odot} \leq M_{\text{ZAMS}} \leq 90M_{\odot}$  and effective temperatures  $T_{\text{eff}} \leq 10^4\text{K}$  are stable against radial oscillations during  $\approx 95\%$  of the time needed to move along the loop of the evolutionary track. The stability against radial oscillations is due to the strong convection in helium ionization zones which suppresses the  $\kappa$ -mechanism of pulsation instability, whereas the zone of the iron Z-bump locates too deep in the stellar envelope and does not play any perceptible role. Therefore, radial pulsations of yellow hypergiants take place only in the beginning and in the end of this evolutionary stage.

Estimates of the upper limit of period of radially pulsating hypergiants obtained in the present study can be applied to interpretation of some variable stars. For example, semi-regular light variations of  $\rho$  Cas with period of 300 day  $\lesssim \Pi \lesssim 500$  day definitely cannot be explained in terms of radial stellar oscillations. Another example is the pulsating variable star V1427 Aql with uncertain evolutionary status. In some studies this variable is discussed as the post-AGB stars, whereas in other works as a yellow hypergiant (see, for discussion, Le Coroller et al. 2003). Multicolor photometric observations of V1427 Aql carried out during eight years reveal the presence of light variations with periods of 130 and 200 day, the star moving blueward in the HR diagram (Archipova et al. 2009). Results of our computations allow us to conclude that V1427 Aql is rather the post-AGB star because assumption on yellow hypergiant leads to following contradictions. First, the mean effective temperature of this star is  $T_{\text{eff}} = 6750\text{K}$  (Kipper 2008) and corresponds to the region of pulsational stability. Second, the period of light changes  $\approx 200$  day significantly exceeds its upper limit for radially pulsating yellow hypergiants evolving blueward in the HR diagram.

Discussed above results of hydrodynamic calculations deal with massive stars with effective temperatures  $T_{\text{eff}} \leq 10^4\text{K}$ . In the present study we carried out hydrodynamic computations for some models with higher effective temperatures corresponding to the both earlier and later stages of stellar evolution. In the first case pulsational instability allows us to conclude that radial oscillations of main-sequence stars with initial mass  $M_{\text{ZAMS}} > 60M_{\odot}$  (Fadееv 2011) exist during the post-main-sequence stage and decay only at effective temperature  $T_{\text{eff}} \approx 7000\text{K}$  due to convection. In the second case radial oscillations arise at the final stage of the yellow hypergiant and do not decay up to exhaustion of helium in the stellar core. With increasing effective temperature the hypergiant becomes the LBV-star radial pulsations of which are responsible for the microvariability (Fadееv 2010) and then transforms into the Wolf-Rayet star which is also pulsationally unstable (Fadееv 2007, 2008a, 2008b).

## REFERENCES

1. A. Arellano Ferro, MNRAS **216**, 571 (1985).
2. V.P. Arkhipova, V.F. Esipov, N.P. Ikonnikova, G.V. Komissarova, A.M. Tatarnikov, B.F. Yudin, Pis'ma Astron. Zh., **35**, 846 (2009) [Astron. Lett., **35**, 764 (2009)].
3. E. Böhm–Vitense, Zeitschrift für Astrophys. **46**, 108 (1958).
4. H. Le Coroller, A. Lébre, D. Gillet, et al., Astron. Astrophys. **400**, 613 (2003).
5. Yu.A. Fadeyev, Pis'ma Astron. Zh., **33**, 775 (2007) [Astron. Lett. **33**, 692 (2007)].
6. Yu.A. Fadeyev, Astron. Zh. **85**, 716 (2008a) [Astron. Rep. **54**, 645 (2008)].
7. Yu.A. Fadeyev, Pis'ma Astron. Zh., **34**, 854 (2008b) [Astron. Lett. **34**, 772 (2008)].
8. Yu.A. Fadeyev, Pis'ma Astron. Zh., **36**, 380 (2010) [Astron. Lett. **36**, 362 (2010)].
9. Yu.A. Fadeyev, Pis'ma Astron. Zh., **37**, 13 (2011) [Astron. Lett. **37**, 11 (2011)].
10. M. W. Feast and A. D. Thackeray, MNRAS **116**, 41 (1956).
11. N. Gorlova, A. Lobel, A.J. Burgasser, et al.), Astrophys.J **651**, 1130 (2006).
12. C. de Jager, *The Brightest Stars* (Reidel, Dordrecht, 1980; Mir, Moscow, 1984).
13. C. de Jager, Astron. Astrophys. Rev. **8**, 145 (1998).
14. C. de Jager and H. Nieuwenhuijzen, MNRAS **290**, L50 (1997).
15. C. de Jager, A. Lobel, H. Nieuwenhuijzen, et al., MNRAS **327**, 452 (2001).
16. T. Kipper, Baltic Astron. **17**, 87 (2008).
17. R. Kuhfuss, Astron. Astrophys. **160**, 116 (1986).
18. N. Langer, C.A. Norman, A. de Koter, et al., Astron. Astrophys. **475**, L19 (2007).
19. A. Lobel, C. de Jager, H. Nieuwenhuijzen, et al., Astron. Astrophys **291**, 226 (1994).
20. A. Lobel, G. Israelian, C. de Jager, et al., Astron. Astrophys. **330**, 659 (1998).
21. G. Meynet, A. Maeder, G. Schaller, et al., Astron. Astrophys. Suppl. **103**, 97 (1994).
22. E.A. Olivier and P.R. Wood, MNRAS **362**, 1396 (2005).
23. R.D. Richtmyer and K.W. Morton, *Difference Methods for Initial–Value Problems* (2nd ed., Interscience, 1967; Mir, Moscow, 1972).

24. Y. Sheffer and D. L. Lambert, PASP **98**, 914 (1986).
25. R. Smolec and P. Moskalik, Acta Astron. **58**, 193 (2008).
26. R.B. Stothers, Astrophys. J. **589**, 960 (2003).
27. R.B. Stothers and C.-W. Chin, Astrophys. J. **468**, 842 (1996).
28. R.B. Stothers and C.-W. Chin, Astrophys. J. **560**, 934 (2001).
29. E. Zsoldos and J. B. Percy, Astron. Astrophys. **246**, 441 (1991).
30. G. Wuchterl and M.U. Feuchtinger, Astron. Astrophys. **340**, 419 (1998).

Hydrodynamic models of yellow hypergiants

$M_{\text{ZAMS}}/M_{\odot}$	$M/M_{\odot}$	$L/L_{\odot},$ $10^6$	$X_{\text{s}}$	$T_{\text{eff}},$ $10^3\text{K}$	$\Pi,$ day	$Q,$ day	$k$	$\dot{\Pi}/\Pi$ $10^{-5} \text{ day}^{-1}$	$\Delta R/R$	$\Delta U,$ km/s
65	32.9	1.03	0.24	10	63	0.0587	0	3.6	0.65	140
				9	82	0.0551	0	3.6	0.28	79
				8	115	0.0541	0	2.4	0.33	84
				7	168	0.0525	0	1.3	0.33	77
				6.8	180	0.0516	0		0.28	60
	28.6	1.08	0.10	7.5	110	0.0380	1	-0.44	0.08	25
				8	124	0.0523	0	-0.60	0.37	92
				9	87	0.0524	0	-0.60	0.31	86
				10	64	0.0525	0		0.28	87
90	42.2	1.52	0.16	10	74	0.0584	0		0.42	110
				9	100	0.0559	0	2.5	0.32	91
				8	143	0.0561	0		0.39	101
				7.5	124	0.0402	1	1.5	0.09	27
	38.4	1.52	0.08	7.7	123	0.0413	1		0.07	19
				8	111	0.0421	1	-0.44	0.14	49
				9	103	0.0553	0	-0.63	0.36	101
				10	76	0.0563	0		0.31	100

## FIGURE CAPTIONS

- Fig. 1. (a) – Parts of the evolutionary tracks of stars with initial mass  $M_{\text{ZAMS}} = 90M_{\odot}$  (solid line) and  $M_{\text{ZAMS}} = 65M_{\odot}$  (dashed line) during the post-main-sequence core contraction. Arrows indicate the direction of evolution along the track. (b) – The rate of effective temperature change  $d \ln T_{\text{eff}}/dt$  along the track.
- Fig. 2. The amplitude of the radial displacement of the outer boundary  $\Delta R/R$  (a) and the period of radial pulsations  $\Pi$  (b) as a function of the effective temperature  $T_{\text{eff}}$  for models of the evolutionary sequence  $M_{\text{ZAMS}} = 65M_{\odot}$ . Dashed lines correspond to the evolutionary expansion of outer layers of the star and solid lines correspond to their contraction.
- Fig. 3. The normalized mechanical work over a closed thermodynamic cycle  $W_j$  as a function of the relative equilibrium radius  $r/R$  at the evolutionary stage of expansion of outer layers of the star  $M_{\text{ZAMS}} = 65M_{\odot}$  at effective temperature  $T_{\text{eff}} = 10^4\text{K}$  (solid line) and  $T_{\text{eff}} = 6800\text{K}$  (dashed line).
- Fig. 4. Same as in Fig. 3 but for the evolutionary stage of contraction of outer layers of the star with  $T_{\text{eff}} = 7400\text{K}$  (dashed line) and  $T_{\text{eff}} = 10^4\text{K}$  (solid line).
- Fig. 5. The gas flow velocity at the outer boundary  $U$  (a) and the light in V band  $m_V$  (b) of hydrodynamic models of the hypergiant with initial mass  $M_{\text{ZAMS}} = 65M_{\odot}$  and effective temperature  $T_{\text{eff}} = 7500\text{K}$ . Solid and dashed lines correspond to evolutionary stages of contraction and expansion, respectively.
- Fig. 6. Same as in Fig. 5 but for hydrodynamical models of the hypergiant with effective temperature  $T_{\text{eff}} = 8000\text{K}$ .
- Fig. 7. Same as in Fig. 2 but for hypergiants with initial mass  $M_{\text{ZAMS}} = 90M_{\odot}$ .

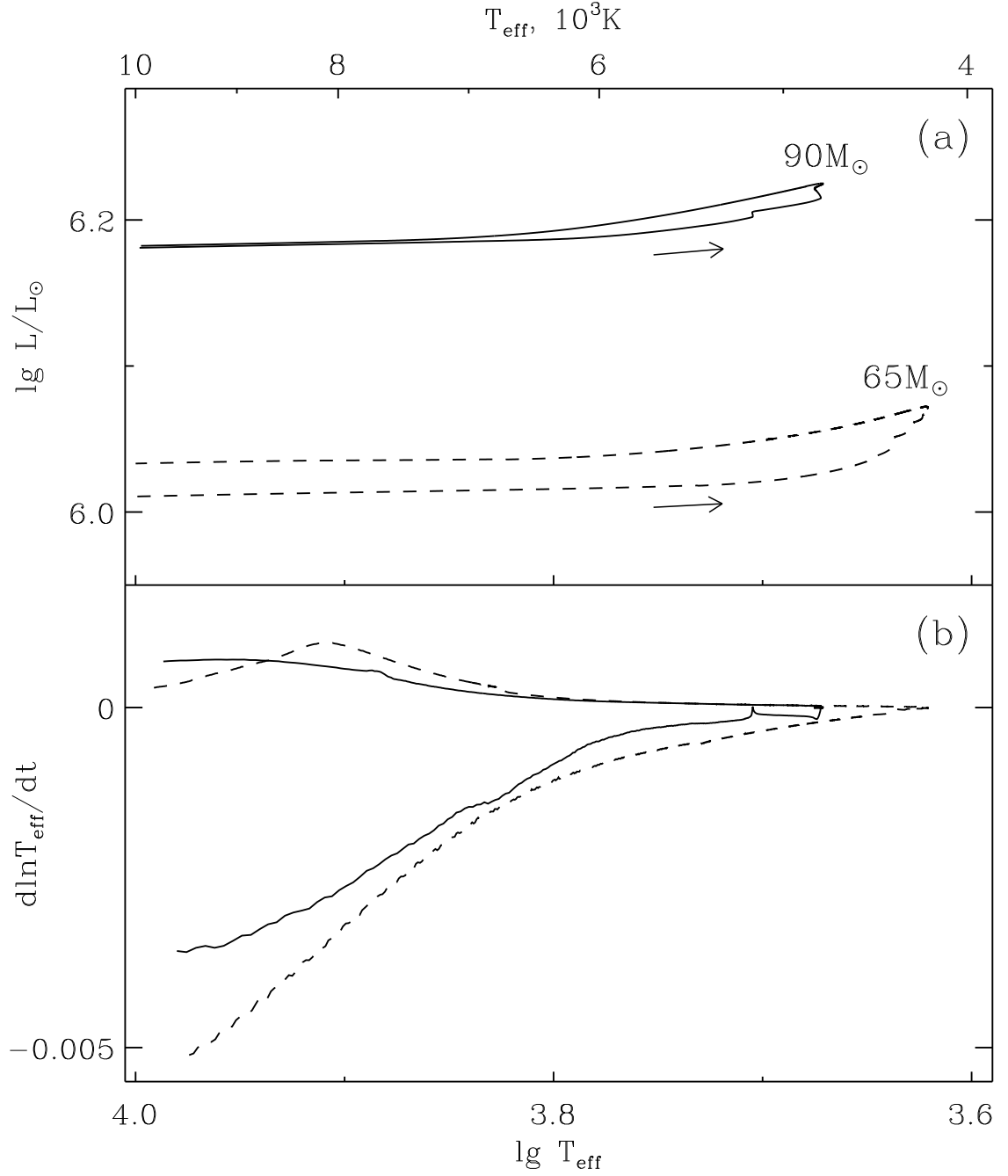


Figure 1: (a) – Parts of the evolutionary tracks of stars with initial mass  $M_{\text{ZAMS}} = 90M_\odot$  (solid line)  $M_{\text{ZAMS}} = 65M_\odot$  (dashed line) during the post-main-sequence core contraction. Arrows indicate the direction of evolution along the track. (b) – The rate of effective temperature change  $d \ln T_{\text{eff}} / dt$  along the track.

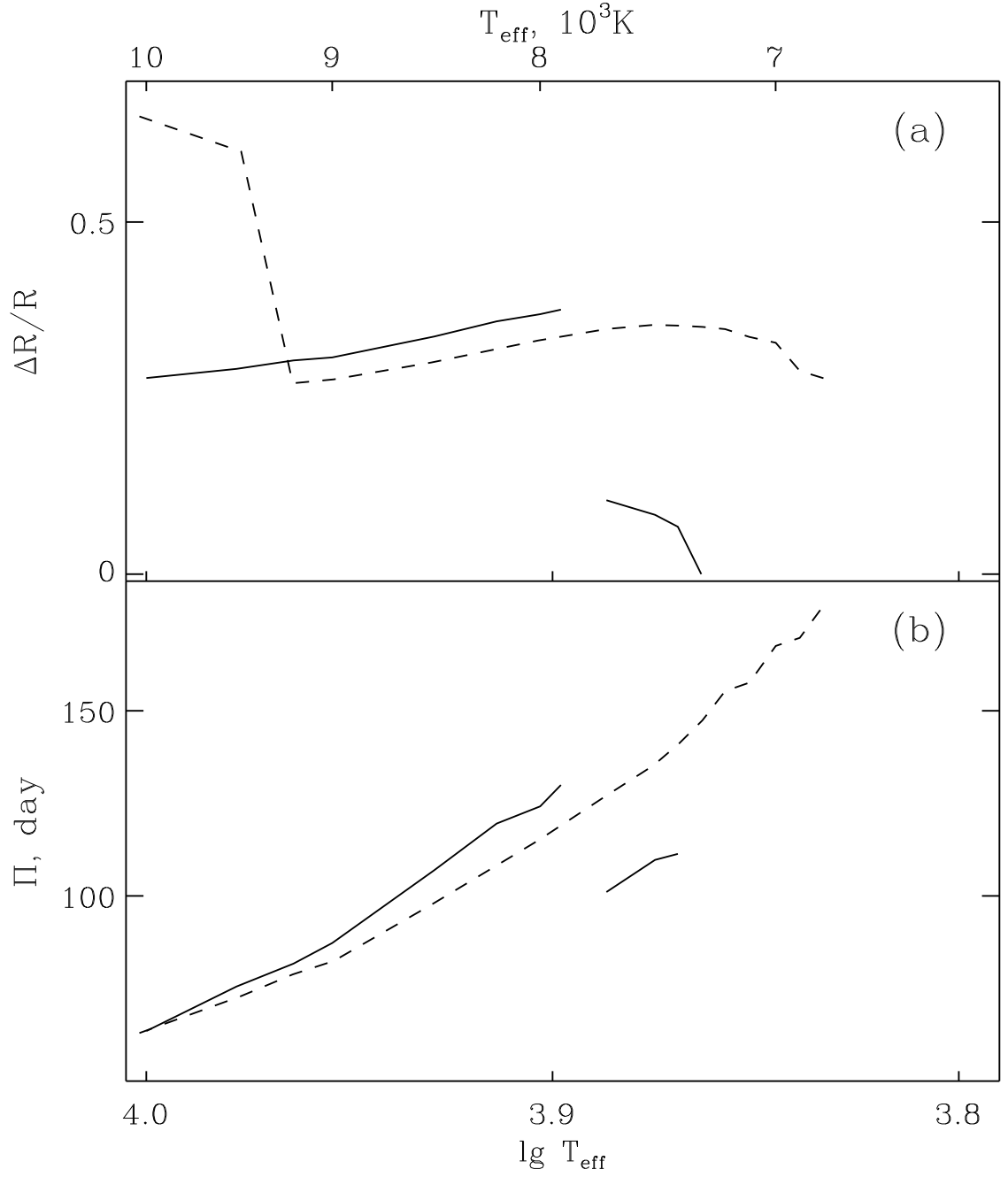


Figure 2: The amplitude of the radial displacement of the outer boundary  $\Delta R/R$  (a) and the period of radial pulsations  $\Pi$  (b) as a function of the effective temperature  $T_{\text{eff}}$  for models of the evolutionary sequence  $M_{\text{ZAMS}} = 65M_{\odot}$ . Dashed lines correspond to the evolutionary expansion of outer layers of the star and solid lines correspond to their contraction.

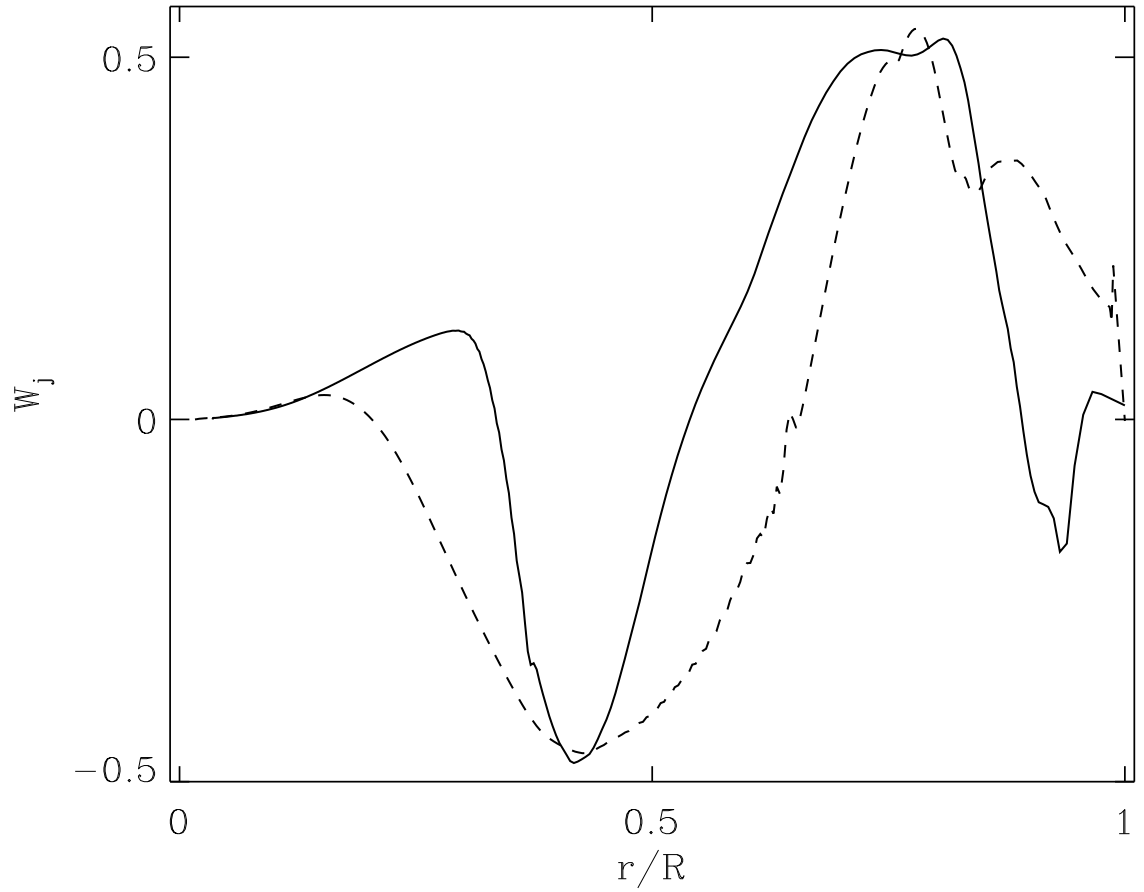


Figure 3: The normalized mechanical work over a closed thermodynamic cycle  $W_j$  as a function of the relative equilibrium radius  $r/R$  at the evolutionary stage of expansion of outer layers of the star  $M_{\text{ZAMS}} = 65M_{\odot}$  at effective temperature  $T_{\text{eff}} = 10^4 \text{ K}$  (solid line) and  $T_{\text{eff}} = 6800 \text{ K}$  (dashed line).



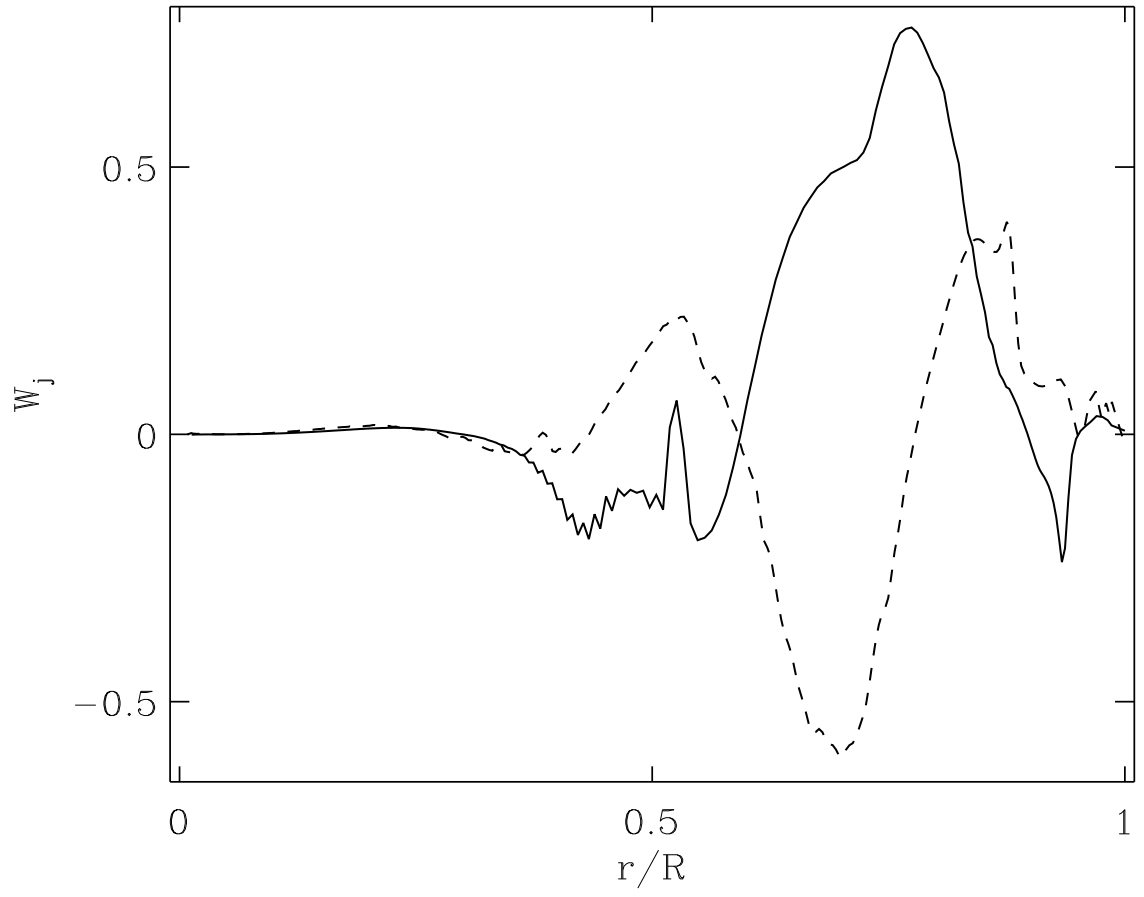


Figure 4: Same as in Fig. 3 but for the evolutionary stage of contraction of outer layers of the star with  $T_{\text{eff}} = 7400 \text{ K}$  (dashed line) and  $T_{\text{eff}} = 10^4 \text{ K}$  (solid line).

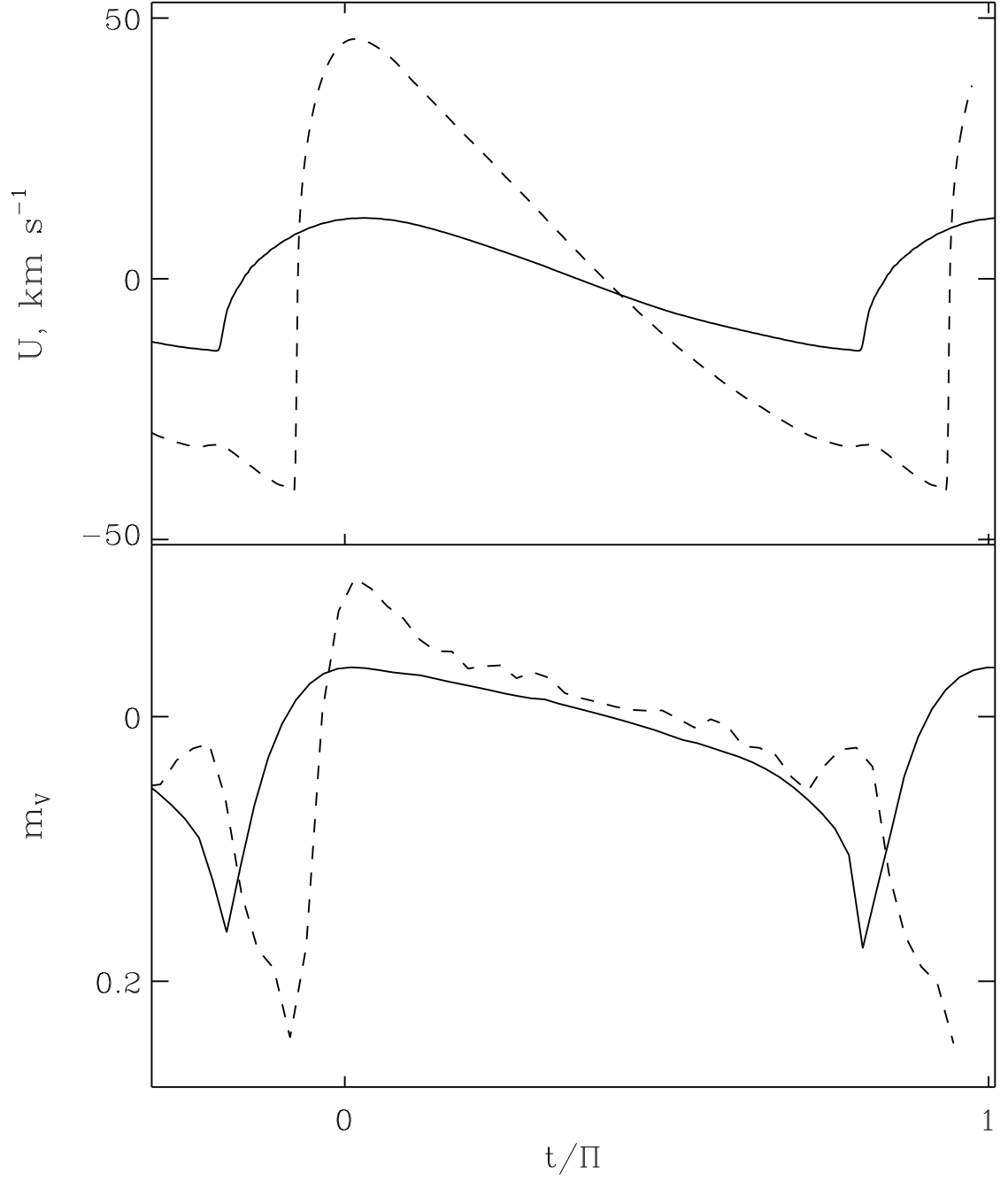


Figure 5: The gas flow velocity at the outer boundary  $U$  (a) and the light in V band  $m_V$  (b) of hydrodynamic models of the hypergiant with initial mass  $M_{\text{ZAMS}} = 65M_{\odot}$  and effective temperature  $T_{\text{eff}} = 7500\text{K}$ . Solid and dashed lines correspond to evolutionary stages of contraction and expansion, respectively.

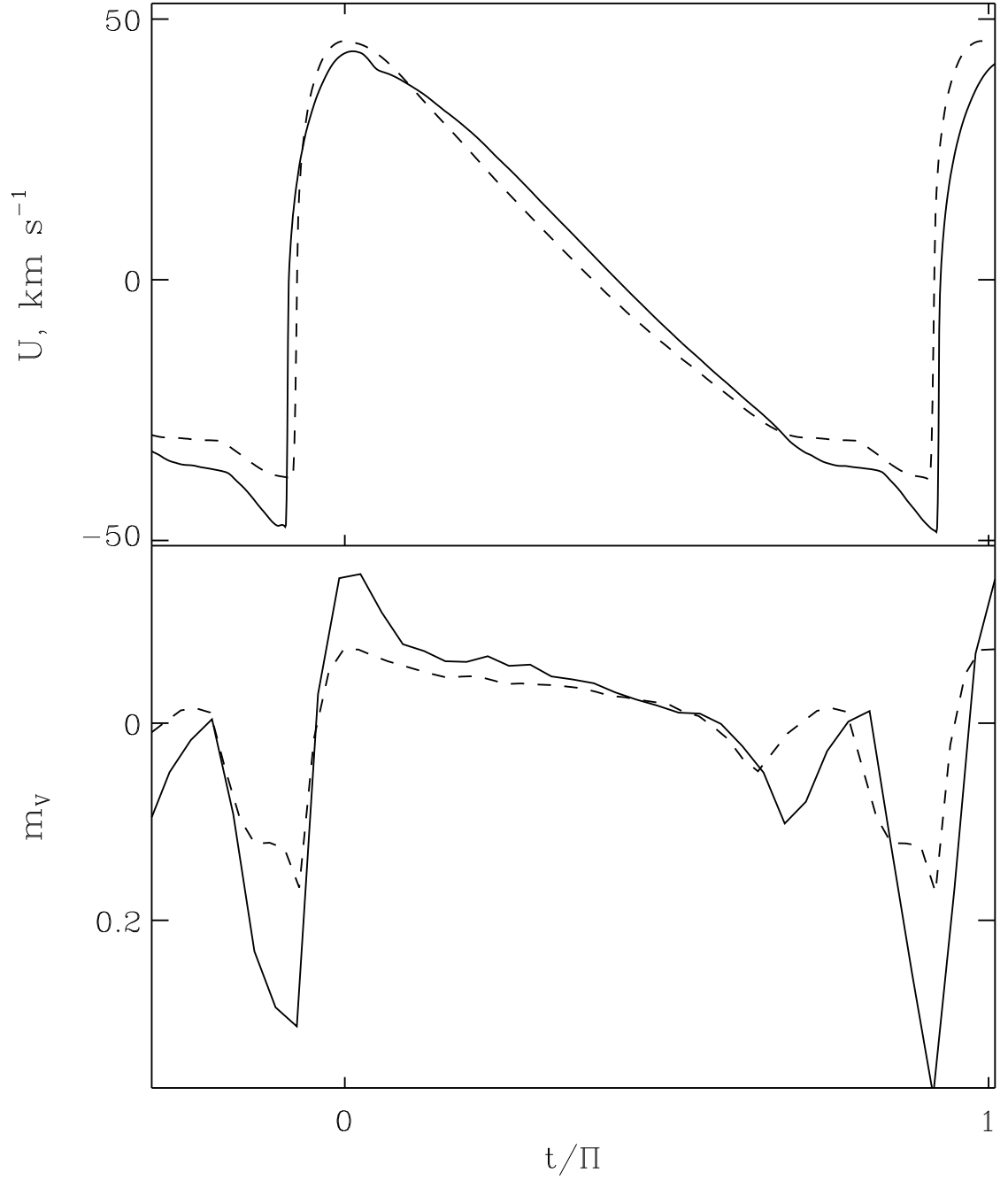


Figure 6: Same as in Fig. 5 but for hydrodynamical models of the hypergiant with effective temperature  $T_{\text{eff}} = 8000\text{K}$ .

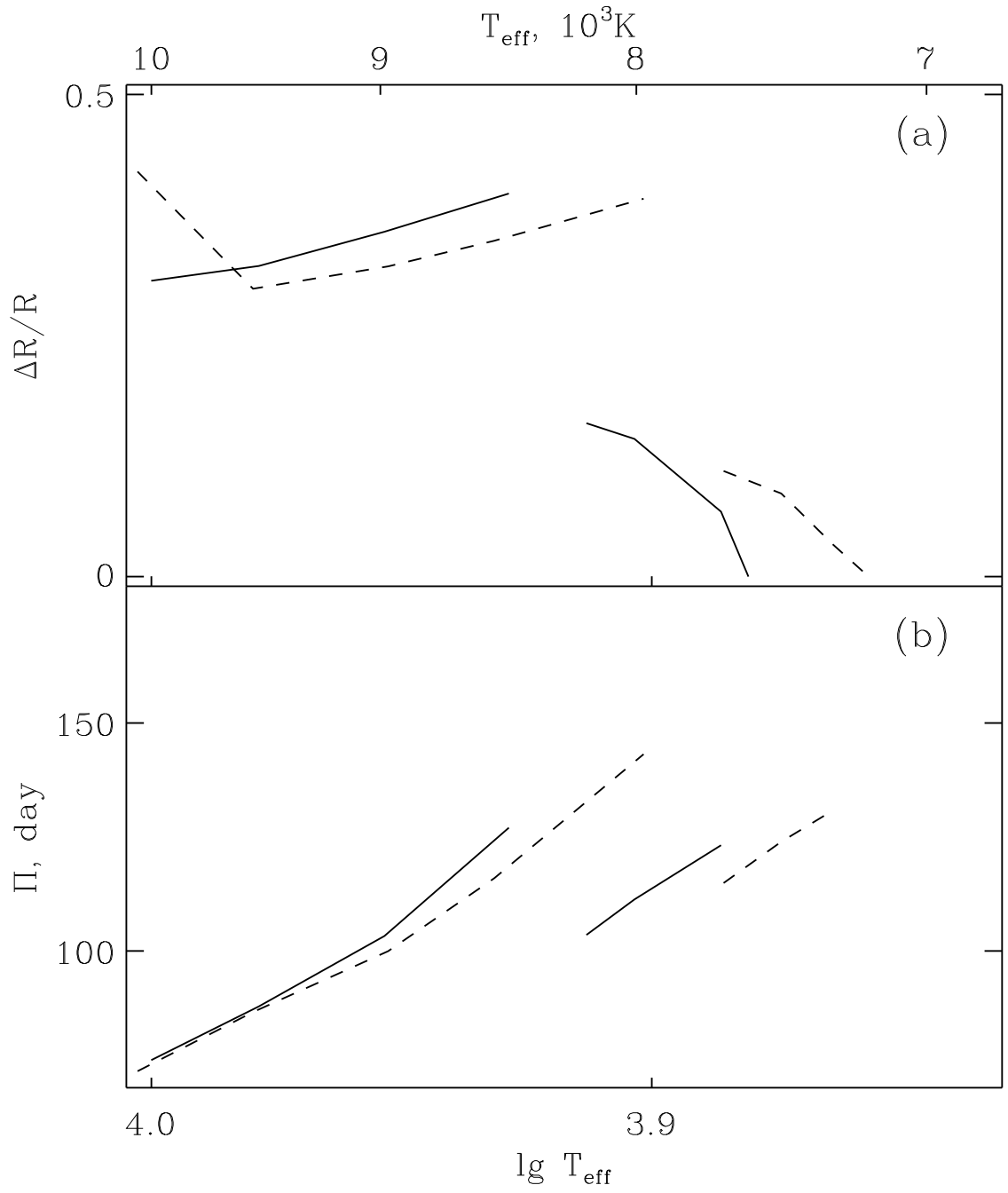


Figure 7: Same as in Fig. 2 but for hypergiants with initial mass  $M_{\text{ZAMS}} = 90M_{\odot}$ .